Combustion and Flame 230 (2021) 111437

Contents lists available at ScienceDirect

Combustion and Flame

journal homepage: www.elsevier.com/locate/combustflame

Simultaneous high-speed spectroscopy and 2-color pyrometry analysis in an optical compression ignition engine fueled with OME_X-diesel blends

José V. Pastor, Antonio García, Carlos Micó*, Felipe Lewiski

CMT - Motores Térmicos, Universitat Politècnica de València, Camino de Vera s/n, 46022 Valencia, Spain

ARTICLE INFO

Article history:
Received 17 September 2020
Revised 16 March 2021
Accepted 24 March 2021
Available online 18 April 2021

Keywords:
E-fuels
Soot
Spectroscopy
Compression ignition

ABSTRACT

E-fuels are a very attractive way for improving the well-to-wheel emissions of CO_2 in internal combustion engines. In the particular case of compression ignition engines, the Oxymethylene dimethyl ether (OME_X), an e-fuel with nearly soot-free combustion under mixing-controlled conditions, is a good candidate for the replacement of fossil fuels. However, the Lower Heating Value of OME_X is nearly half of the diesel fuel, which means that much longer injection durations are required in the real engine. In addition, the very low viscosity and lubricity of OME_X can damage the injection system if used pure, but it can be an interesting fuel when blended with conventional diesel. Thus, the main objective of this paper is to evaluate the potential of OME_X-diesel blends to bypass these OME_X limitations whilst keeping low soot formation trends. For this purpose, a single cylinder optical diesel engine at part load was employed. The soot production for the different fuel blends was analyzed by applying three different high-speed imaging techniques: natural luminosity, flame spectroscopy and 2-color pyrometry. Natural luminosity analysis showed that the flame light intensity scales with diesel fraction up to 30% of diesel in the blend. The spectroscopy analysis has revealed that soot formation of OME_X fuel is almost null. When blended with diesel at 50%, although soot formation is still lower than for pure diesel, higher soot levels are obtained in the last stages of the cycle as a consequence of the longer injections required.

© 2021 The Authors. Published by Elsevier Inc. on behalf of The Combustion Institute.
This is an open access article under the CC BY license (http://creativecommons.org/licenses/by/4.0/)

1. Introduction

It is well known that the transportation sector is constantly evolving towards a cleaner propulsion systems. Regarding light duty vehicles, the utilization of hybrid and electric technologies in replacement of the internal combustion engines [1] has taken great relevance. In contrast, regarding medium and heavy-duty applications, the current scenario points to a long life for the diesel engines. This statement can be based on the high efficiency of this technology as well as the dynamism and energy density provided, which are important factors for this kind of activities (e. g., freight transport).

In this context, it is of big interest for researchers and the automotive industries to find new solutions for pollutant reduction and efficiency improvements in ICEs. In this scenario, renewable fuels have been considered as an alternative to achieve both cleaner combustion and fossil-fuel dependency reduction. Among these fuels, it can be highlighted the biofuels and e-fuels. Biofuels are produced from the biomass or organic matter. In contrast, e -fuels are synthetic fuels which are produced using renewable energy and do not compete with foodstuffs, as they use CO_2 as raw material. They are considered as a promising way to chase carbon neutrality, drastically reducing the footprint of vehicles from its life-cycle perspective [2].

Among the e-fuel types, synthetic oxygenated fuels as the Oxymethylene dimethyl ethers present interesting characteristics. OME_X are C_1-oxygenated fuels with the molecular structure CH3-O-(CH2-O)x-CH3, where x represents the chain length. As it increases, the oxygen content, density and cetane number also increase [3]. These molecules do not have direct carbon bonds (C–C) [3] which, in combination with the oxygen content, provide low or even negligible soot emissions [4]. During the first stages of combustion, OME_X forms hydroperoxides, which are decomposed in OH-radicals. They promote an oxidation process which brakes the soot precursors [5]. In addition, these fuels allows the utilization of high EGR rates to reduce NO_x emissions without penaliz-

* Corresponding author.
E-mail address: carmirec@mot.upv.es (C. Micó).

https://doi.org/10.1016/j.combustflame.2021.111437
0010-2180/© 2021 The Authors. Published by Elsevier Inc. on behalf of The Combustion Institute. This is an open access article under the CC BY license (http://creativecommons.org/licenses/by/4.0/)

Nomenclature

2C	Two color pyrometry
AFR	Air-fuel ratio
CA50	crank angle when 50% of total heat released is achieved
CAD	Crank angle degree
CI	Compression Ignition
CO_2	Carbon dioxide
C_r	Compression Ratio
EGR	Exhaust Gas Recirculation
FPS	Frames per second
ICE	Internal combustion engines
IMEP	Indicated mean effective pressure
LHV	Low heat Value
NL	Natural Luminosity
NO_X	Nitrogen dioxide and monoxide
OEM	Original Equipment Manufacturer
OME_X	Oxymethylene dimethyl ether
Pinj	Injection pressure
Pint	Intake pressure
RoHR	Rate of heat release
RoHR	Rate of heat release
rpm	engine speed
Tcool	Coolant temperature
Tint	Intake temperature
Toil	Oil temperature
UV	Ultraviolet
WTW	well-to-wheels
O100	Pure OME_X
D100	Pure diesel
O50D50	50% OME_X and 50% diesel
O90D10	90% OME_X and 10% diesel
O80D20	80% OME_X and 20% diesel
O70D30	70% OME_X and 30% diesel

ing in soot formation, which means a reduction of the well-known soot-NO_X trade-off [6].

OME_X presents good characteristics to be directly used in diesel engines without the necessity of fuel injection system modifications [7]. The most similar characteristics to diesel fuel are found for blends of OME_{3-5}, (X varies between 3 and 5) that can be used in a pure liquid form [8]. They offer a high boiling point (no pressurized tank is required) and viscosity when compared to OME_1 and DME (dimethyl ether), for example. The cetane number of OME_{3-5} mixtures is between 70 and 100. It is higher than conventional diesel, which guarantees better ignitability and lower ignition delay [9]. Additionally, OME_X offers a shorter combustion duration than diesel [10]. On one hand, the premixed phase is reduced in comparison with the fossil fuel. Its higher cetane number diminishes the ignition delay and, consequently, the amount of fuel burned during this phase. In combination with a minor lower heating value (LHV), this reduces the maximum rate of heat release (RoHR) peak [11]. On the other hand, during the diffusive phase, OME_X is characterized for promoting faster burn out. During this phase, the high oxygen content in the molecule diminishes the need of oxygen from the air, which improves the oxidation rate [12]. The shorter combustion duration also increases the thermal efficiency, mainly for low and medium engine loads [13]. Regarding pollutant formation, results have shown that soot emission are strongly reduced regardless the AFR used [14,11]. In addition, under EGR conditions, it is possible to decrease the NO_X emissions without impacting soot emissions and achieving the emissions regulations target [15,16]. In addition, it was proved that for longer OME_X chain lengths ($X = 5$), the NO_X emissions are lower [14]. In contrast, the main drawback is the lower LHV of these fuels in comparison to diesel. This makes it necessary to use longer injection durations, which can be problematic for high engine load and speed operating conditions [2].

The potential of OME_X fuels to promote low soot formation and replace the fossil diesel is evident. However, considering its limitations, blending it with diesel seems an attractive solution to increase the fuel LHV while keeping low soot formation levels [7,17]. In this context, the optical techniques allow to provide more insight regarding the chemical and physical processes that govern the OME_X combustion and soot formation. Some optical investigation have been performed in constant volume vessels [8,3] and rapid compression machines [18]. However, these tests are focused on the analysis of spray characteristics. In contrast, research involving combustion of OME_X in facilities like optical engines under real operating conditions, including spray-wall interaction and real flow movement, are very scarce. This kind of studies are extremely important for understanding the combustion process evolution and flame behavior under realistic operating conditions, as well as to corroborate the conclusions reported in previous studies performed in metal engines or optical test rigs.

Considering all the above mentioned, the current study has the objective of studying the soot formation when using different substitution rates of diesel in OME_X, focusing on how the soot formation increases as the diesel content increases in the blend. The present paper aims to fill an important gap regarding the comprehension of the influence of the diesel fraction when it is mixed with OME_X, which promotes low soot formation, under real engine operating conditions.

In previous works [19], it has been observed that the OME_X flame emits radiation. However, it was not possible to identify if it comes from the soot formation or from the chemiluminescence of chemical species. One possible way for identifying the source is through emissions spectroscopy analysis [20,21], where the species are identified by specific emission wavelengths. In order to address this question and fulfill the objective of this work, different approaches were considered in the study: Natural luminosity imaging, high-speed emissions spectroscopy, 2-color pyrometry and in-cylinder pressure analysis. Neat OME_X, OME_X-diesel blends (O90D10, O80D20, O70D30 and O50D50) and neat diesel were tested and analyzed.

The results have confirmed zero soot formation when the engine was operated with pure OME_X. When it is blended with diesel, this fuel could be added up to 20% of mass substitution rate without significantly increasing soot formation. From 50% of diesel mass, the benefits of OME_X starts to disappear, and the differences between blends of OME_X-diesel and neat diesel become very small.

2. Experimental tools and methodology

2.1. Engine

The experimental tests were performed in an optical diesel engine, as shown in Fig. 1, with a Bowditch design and a cylindrical-shaped bowl piston. Its geometry is summarized in Table 1. The cylinder bore and stroke are based on a 1.6 L GM commercial diesel engine. The engine is also equipped with the GM commercial cylinder head, with a centrally positioned injector with 8 holes. Additionally, the cylinder head includes 2 intake valves and 2 exhaust valves per cylinder. A conventional high-pressure pump and common rail are used for the injection system. A DRIVVEN® control unit drives the injector and controls the fuel injection and number of injections per cycle. The optical access to the combustion chamber is achieved through a quartz window located at piston bottom. The window is made of Suprasil 1 fused silica. In or-

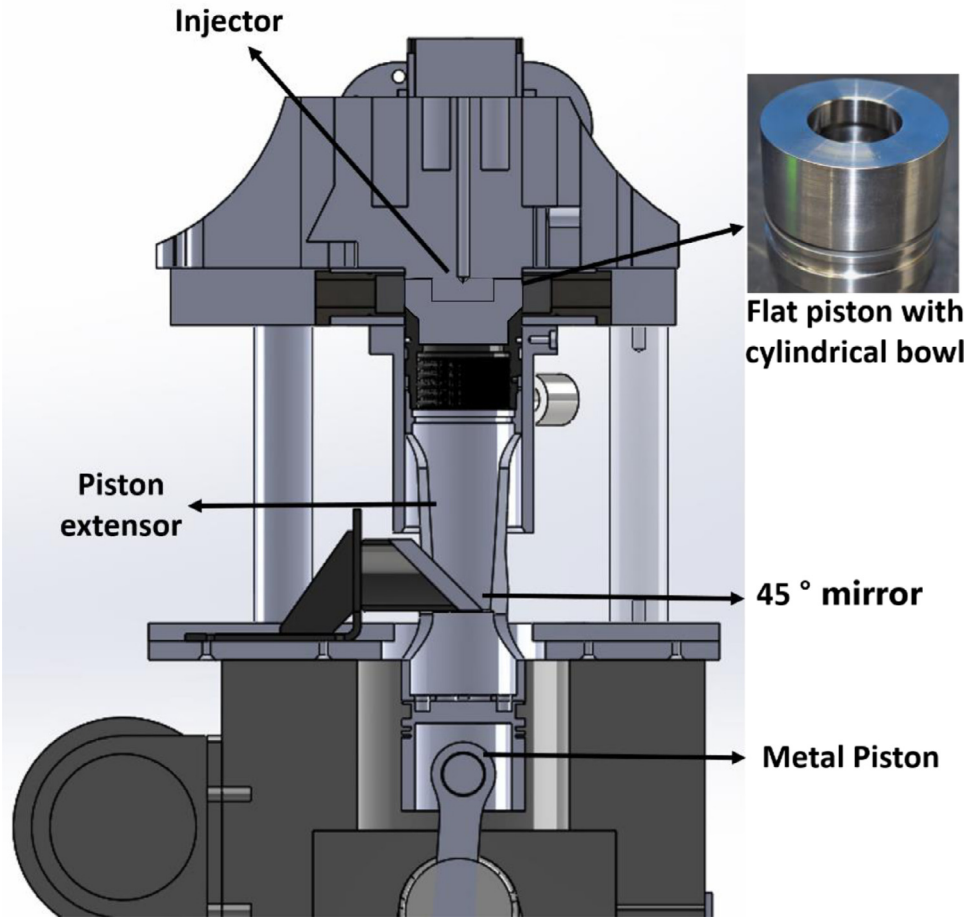

Fig. 1. Optical engine parts.

Table 1
Optical engine characteristics.

Engine type	4 stroke, direct injection
Number of cylinders [-]	1
Number of Valves [-]	4
Bore [mm]	80
Stroke [mm]	80.1
C_r [-]	11
Displacement [l]	0.402

der to reduce the optical access fouling and prevent thermal stress, experiments were performed using a skip-fire strategy (allowed by the control unit). Fuel was injected 1 out of 20 cycles.

The instantaneous intake and exhaust pressure were measured with a piezoresistive transducer (Kistler-4603B10). The in-cylinder pressure was obtained by using a piezoelectric transducer (AVL/GH13P), which was installed in the glow plug holder of the cylinder head. The transducers were connected to a charge amplifier (Kistler 4603B10). An oscilloscope (Yokogawa DL708E) was used for recording the pressure signal, which was synchronized with a crankshaft encoder, with 0.2 CAD resolution. A home-built acquisition system, named SAMARUC, was used for the acquisition of mean variables such as mass air flow, intake and exhaust temperature, oil temperature, etc. The Table 2 represents the accuracy of the different devices used for the experiments. A screw compressor provided the intake air at the required pressure and a valve located at the exhaust system simulated the backpressure. Before the intake air enters the cylinder, it is conditioned by a dryer and a heat exchanger. Additionally, the required intake air temperature is ensured by an air heater located just before the intake port.

2.2. Optical measurements

Spectroscopy in the UV–visible range and flame natural luminosity imaging techniques were applied for the current study. The optical assembly setup is presented in Fig. 2. The flame radiation that comes from combustion chamber goes through the transparent piston bowl and gets reflected by the 45^0 elliptical mirror. The surface of the 45° optical mirror used to look through the piston bottom access is made of enhanced aluminum, which is specified to offer a good reflection efficiency in the UV and the visible range. The mirror ensures a reflection efficiency above 85% between 250 and 700 nm. Then, radiation reaches a quartz neutral density filter. It is made of fused silica with an optical density of 0.15. This filter reflects a small fraction (15%) of the incident light towards a high-speed camera to record the flame natural luminosity images. Most part of the incident light is transmitted (70%) to the spectrograph in the VIS-UV range. This configuration allowed to obtain natural luminosity images and the spectrum measurements simultaneously. For each experiment, 15 combustion cycles were registered. This was conditioned by the piston fouling caused by soot.

Table 2
Accuracy of the sensors.

Variable	Device	Manufacturer / model	Accuracy
In-cylinder pressure	Piezoelectric transducer	AVL / GH13P	±1.25 bar
Intake/exhaust pressure	Piezorresistive transducers	Kistler /4045A10	±25 mbar
Temperature in settling chambers and manifolds	Thermocouple	TC direct / type K	±2.5 °C
Crank angle, engine speed	Encoder	AVL / 364	±0.02 CAD
Air mass flow	Air flow meter	Sensyflow / FTM700-P	< ±1%

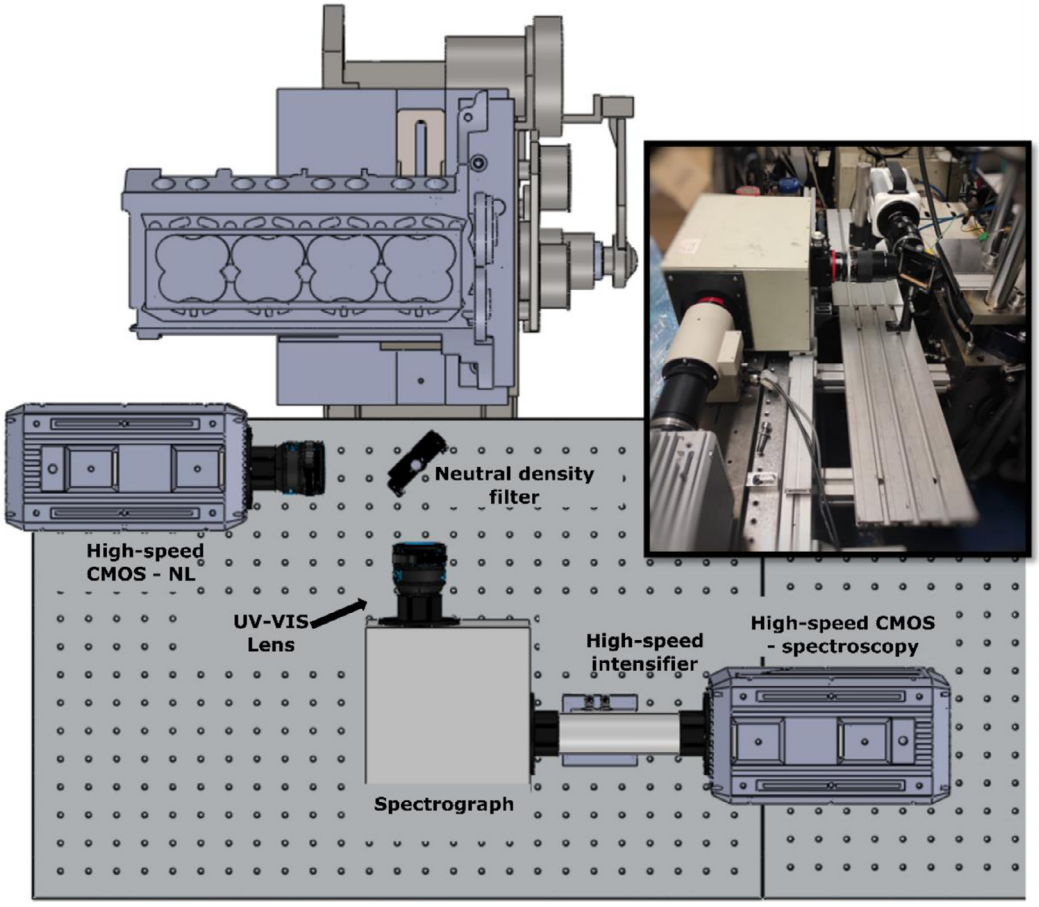

Fig. 2. Optical assembly.

The neat diesel was the most critical fuel in this sense, hindering measurements above 15 combustion cycles.

A Photron Fastcam Nova – S9 (high-speed CMOS) was used for registering the natural luminosity of the flame. A Carl Zeiss Makro-Planar T 100 mm f/2 ZF2 lens was assembled to the camera. It was set to record at 10,000 fps (approx. 0.5 CAD resolution at 1250 rpm of engine speed) with an image size of 640 × 944 pixels. Different exposure times were employed for each fuel blend tested to prevent image saturation. The exposure times were reported in Table 3. An intensity correction was applied during the image post-processing to correct these differences. The image acquisition was triggered with the injection electric pulse.

For the high-speed spectroscopy acquisition, a Jobin Yvon Horiba 180 spectrograph coupled with a Hamamatsu C10880–03F high-speed intensifier and a Photron SA5 Fastcam (high-speed CMOS) were used. The spectrograph was equipped with 600 groove/mm grating. The camera was set to record at 10,000 fps with an image size of 896 × 848 pixels. The different values of gain and exposure time are represented in Table 3. This provided a wavelength bandwidth of 170 nm per image. Thus, in order to cover the desired spectrum range, measurements were performed with the grating centered at three different wavelengths: 330 nm (245–415), 400 nm (315–485) and 470 nm (385–555) respectively. The entrance slit width was set to 0.1 mm for an optimum combination between light intensity and a good spectral resolution. The flame radiation from the combustion chamber was focused with a

Table 3
Shutter speed and gain used for the different fuel blends.

	Fuel	Shutter speed [μs]	Gain (999 max.)
Spectroscopy camera	O100	99.75	850
	O90D10	99.75	850
	O80D20	99.75	850
	O70D30	58.49	850
	O50D50	24.76	850
	D100	39.75	800
Natural Luminosity camera	O100	98	–
	O90D10	14.3	–
	O80D20	1.3	–
	O70D30	0.3	–
	O50D50	0.2	–
	D100	0.2	–

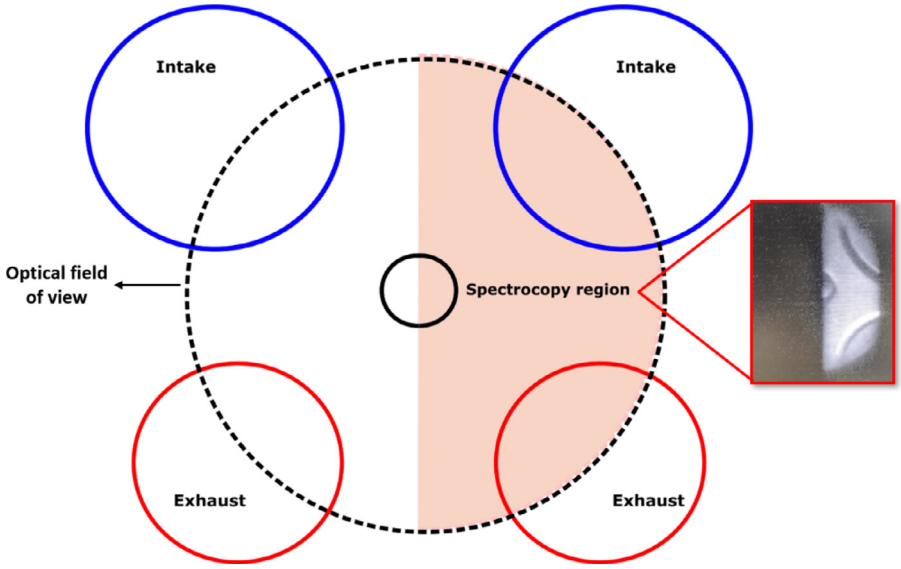

Fig. 3. Combustion chamber region considered for spectroscopy analysis . (For interpretation of the references to colour in this figure legend, the reader is referred to the web version of this article.)

UV Nikon objective (105 mm focal length), coupled to the entrance slit.

The selected slit width resulted in a field of view, which is represented in Fig. 3. The spectroscopy measurement region (highlighted) includes half of the bowl. An image from the field of view was acquired based on the "zero order" diffraction of the grating. In this configuration, the radiation is not decomposed per wavelengths and a conventional image is obtained. When radiation is decomposed, the spectrum is split along the horizontal axis of the image while the vertical axis corresponds to the vertical location within the field of view.

A calibration was performed by using a mercury-argon light source with a known discrete emission spectrum. During this first step, each horizontal pixel of the registered spectra was converted to a specific wavelength. In addition, as the grating efficiency varies with the wavelength, a second correction of the spectra intensity was performed to compensate this effect. As a reference, a tungsten-ribbon calibration lamp, with a known continuous emission spectrum [22], was used. For each recorded instant, a mean intensity value per wavelength (horizontal axis) was calculated considering only the pixels (in the vertical axis) corresponding to the measurement region shown in Fig. 3.

The tungsten-ribbon lamp allows also to calibrate the system to transform digital levels to light intensity of radiation (W/(sr m^2nm)). This information has been used to perform a similar analysis to the one characteristic of 2-Color pyrometry [19,23]. By using the light intensity of two different wavelengths, the Planck law and the soot emissivity equations can be solved and the soot KL factor (optical density) as well as the soot temperature can be calculated. The wavelengths 450 and 530 nm were used for the 2C analysis. The first one is large enough to guarantee a small influence of the chemiluminescence radiation of the flame. The second one is separated from the grating edge, where the grating efficiency is poor (and correction is not reliable). The KL values are calculated from the mean intensity of radiation obtained for each wavelength.

2.3. Fuels and operating conditions

Commercial diesel and OME_X, as well as several blends of them, were studied in the current work. The main fuel properties are presented in Table 4. It is important to highlight the differences in terms of LHV, which is much lower for the OME_X, as well as the much higher oxygen content in comparison with diesel. Another important factor is the higher Cetane number for the OME_X, which impacts directly in ignition delay and the energy released during the premixed phase. The blends are in mass and they were obtained by mixing different percentages of diesel in neat OMEX. (10%, 20%, 30% and 50%). The miscibility of diesel and OME_X was analyzed for different percentages. For blends up to 50% of diesel the results were satisfactory. In addition, previous works have already been used the same percentages of diesel blended in OME_X [15,16].

Table 4
Fuel properties.

	EN 590 diesel	OME_X
Density [kg/m^3] (T = 15 °C)	842	1067
Viscosity [mm^2/s] (T = 40 °C)	2.929	1.18
Cetane number [-]	55.7	72.9
Carbon content [% m/m]	86.2	43.6
Hydrogen content [% m/m]	13.8	8.82
Oxygen content [% m/m]	0	47.1
Lower heating value [MJ/kg]	42.44	19.04

The test matrix and engine conditions used in this work are represented in Table 5. Tests were performed at around 9.2 bar IMEP (Fig. 4) and a constant engine speed of 1250 rpm. The injection timing and duration were adjusted for each fuel, trying to keep the same IMEP and similar CA50. All IMEP values are around 9.2 bar with small variations (specially for neat Diesel). However, these conditions have been considered similar enough to perform the comparison of the different fuels tested. The intake pressure and temperature were the same for all tests. Thus, a different injection strategy for each fuel was necessary (Fig. 5). In order to simulate more realistic operating conditions, an exhaust backpressure with 0.2 bar higher than intake pressure was employed. This could be achieved by means of an electronically controlled valve located at the exhaust system. The coolant of the cylinder wall was kept between 15 ^{0}C and 25 ^{0}C. This is necessary for preserving the pistons rings, which are produced from a synthetic material.

A multiple injections strategy with 4 pulses, including two pilot, one main and one post injection, was employed for the current work. In Table 6 is presented the duration of each injection for each fuel blend. For all fuels tested, the injection pressure was

Table 5
Engine test conditions.

Fuel	Inj. Pattern	Engine Speed	Pint (Bar)	Pexh (Bar)	Tint (°C)	Toil (°C)	Tcool (°C)
OME_X Diesel O90/D10 O80/D20 O70/D30 O50/D50	Mult.	1250	2.15	2.35	100	60	15–25

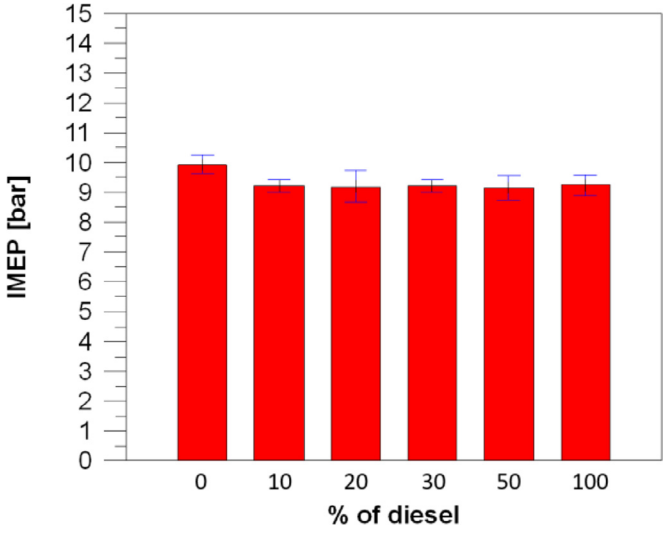

Fig. 4. IMEP for each fuel blend tested -% of diesel in OMEX.

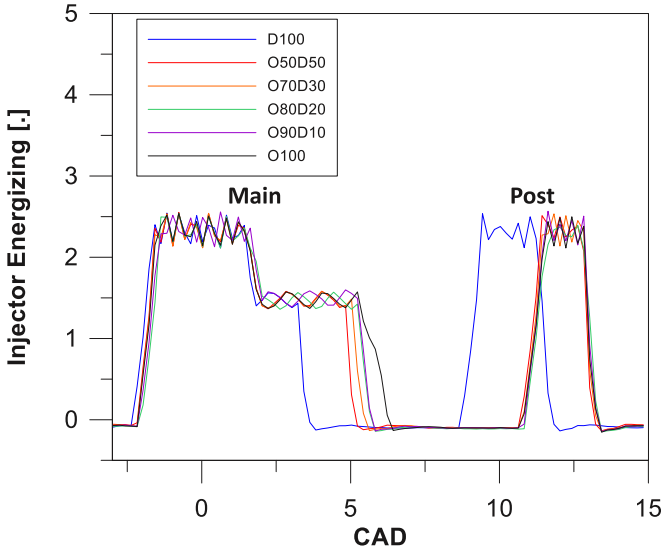

Fig. 5. Injector energizing strategies applied for each blend.

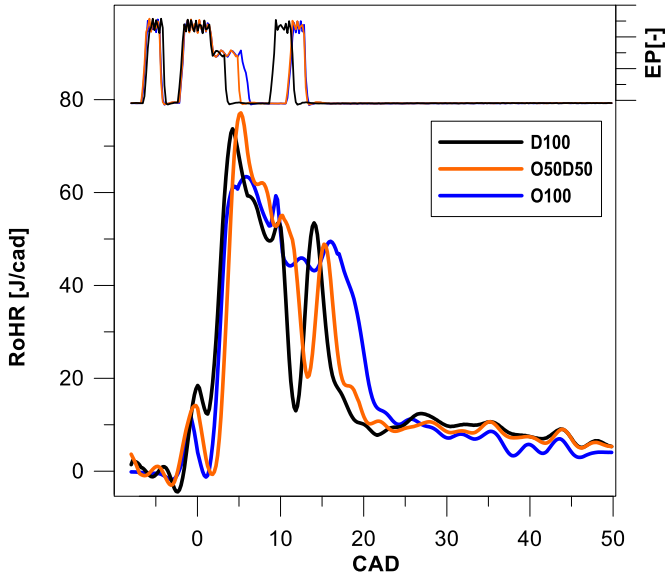

Fig. 6. RoHR for neat OMEX and neat diesel.

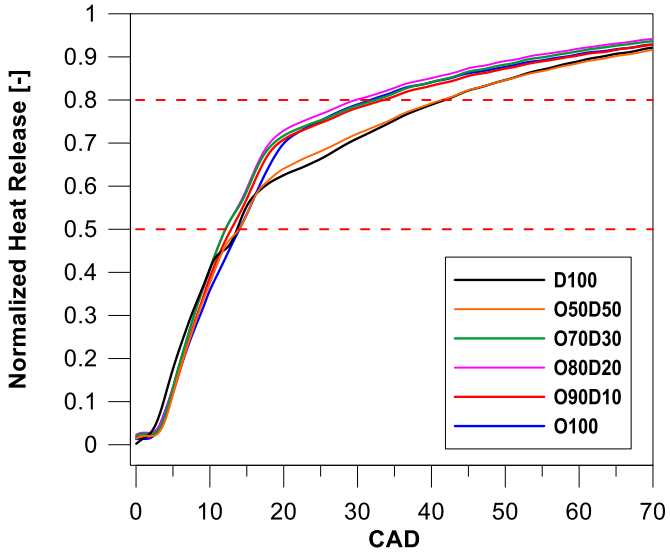

Fig. 7. Cumulative heat release for all fuel blends.

Table 6
Injection durations.

Fuel	Pilot 1 [μs]	Pilot 2 [μs]	Main [μs]	Post [μs]
O100	373	400	1146	373
O90D10	373	400	1065	373
O80D20	373	400	1065	373
O70D30	373	400	1040	373
O50D50	373	400	1013	373
D100	373	400	825	453

kept at 800 bar. The strategy is based on original equipment manufacturer (OEM) used for standard engine calibration. In order to compensate the lower OME_X 's LHV and perform the tests under similar IMEP for all the blends, the energizing timing of the main injection was adjusted for each of them. The Fig. 5 represents the electric pulse only for the main and post injection, where the adjustment is performed.

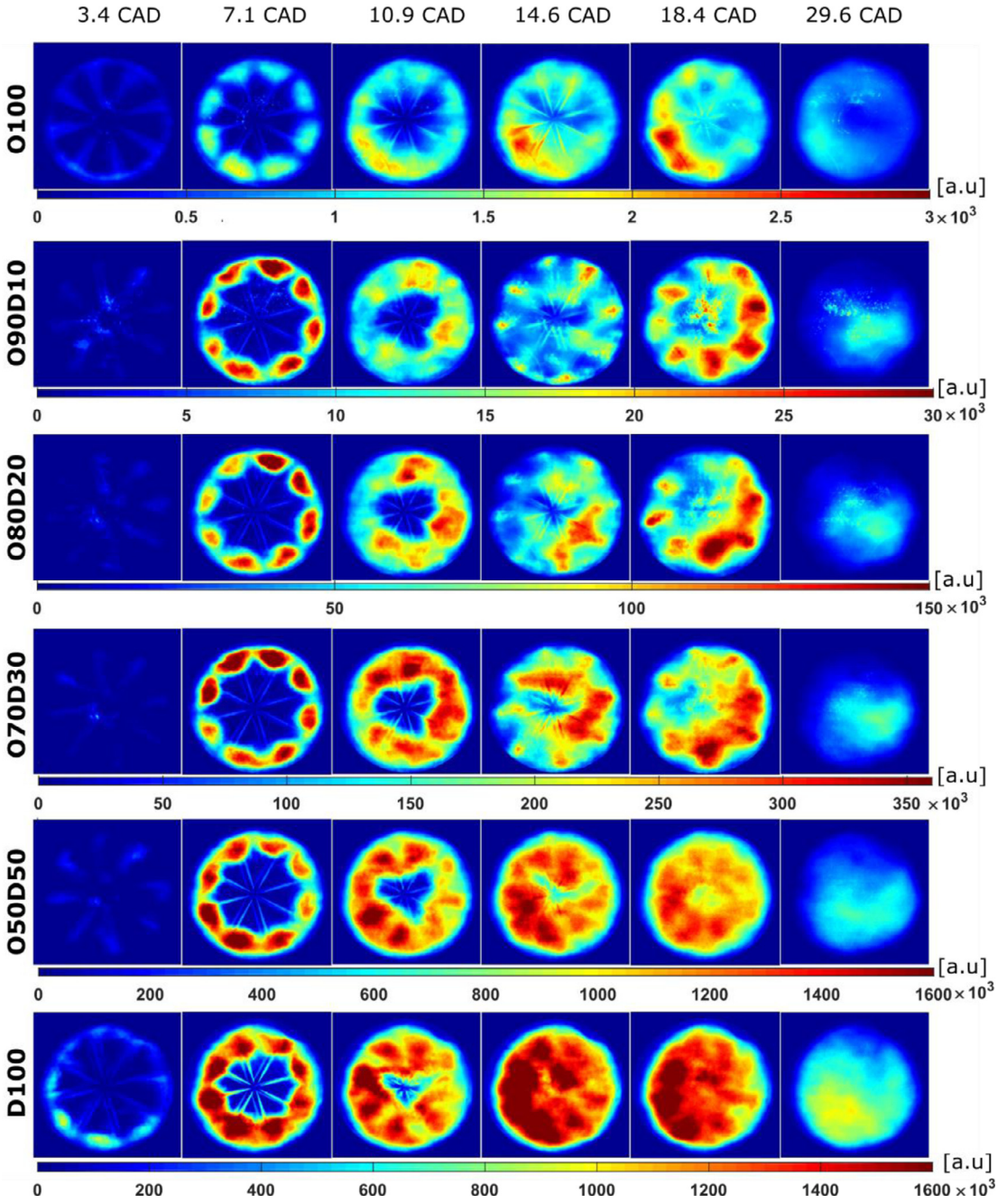

Fig. 8. Flame natural luminosity for each blend tested.

3. Results and discussion

3.1. High speed flame natural luminosity

A first approach has been carried out, based on the flame natural luminosity. It provides less information than other more complex measuring techniques. However, it is still useful to identify differences in terms of flame evolution and radiation between blends. As already discussed by several studies [24,25], the flame light intensity is one of the main indicator of soot concentration. The Figs. 6 and 7, where the RoHR and cumulative HR are shown, will be used to explain and reference the flame events represented in Fig. 8. The RoHR curves were calculated by using a model based on the first law of thermodynamic [26]. In Fig. 8, the flame natural luminosity images for different crank angle degrees and different fuel blends are represented. As it has been mentioned in the previous section, tests for each blend were performed with a different shutter speed configuration, due to the great variation on radiation intensity. Considering this, the measured intensity from each blend was corrected, taking the neat OME_X as reference. In this way, blends and pure fuels can be directly compared. The images at 3.4 CAD represent the premixed combustion phase, where the soot formation rate is low as it is represented by the low radiation intensity observed for all the blends. At 7.1 CAD, combustion achieves the diffusive phase, and the soot formation ratio increases, represented by an important increase of flame broadband radiation. From this point, the differences between blends arise. For all the cases, the highest intensity regions are in the periphery of the bowl, where the flame-flame and flame-wall interactions are occurring. At this instant, the maximum luminosity intensity

increases significantly with diesel fraction, indicating that the soot formation is increasing as well. At 10.9 CAD, the main injection for the blends and neat diesel has finished (not for neat OME_X) and the soot formed begins to be oxidized. For the blends up to 20% of diesel content, the soot generated during the main injection (observed at 7.1 CAD) seems to be oxidized as the radiation observed at 10.9 CAD decreases in comparison with previous instants. The high content of OME_X in the blend could be promoting a faster oxidation of previously formed soot. Above 20% of diesel, in contrast, the trend is the opposite. The radiation intensity is not decreasing and even the area covered by high intensity radiation grows, in comparison with the blends with less diesel fraction. This trend is clearer when moving to 14.6 CAD. At this instant, the blends with lower diesel content (even O70D30) show a clear reduction of radiation intensity in comparison to that measured at 7.1 CAD. However, for O50D50 and neat diesel it seems that soot concentration is still increasing as the high intensity radiation extends to almost the whole piston bowl. Besides, up to 30% of diesel, it is possible to see the jet of the post injection spreading in the flame due to the faster oxidation that occurs during the main injection. In contrast, for O50D50 and D100, the soot cloud remaining inside the bowl still covers the combustion chamber and hides the post injection jets. When the post injection enters in the main injection flame and burns, the light intensity increases considerably. The earlier post injection of D100 could cause a larger increase of the radiation intensity in comparison to the other fuels at 14.6 CAD, but it is considered that this will not alter the soot trend observed when fuels are compared. After that, during the late combustion stage, some differences can be highlighted.

Based on the above mentioned, it can be stated that as the fraction of diesel increases in the blend, the soot oxidation seems to worsen. If the cumulative heat release curve (Fig. 7) is observed, large differences are visible above 50% of total energy released (around 15 CAD). At this stage, the cumulative heat release increases faster for the fuels with high OME_X content and it extends up to the 80% of the total energy released. At first, this behavior could be related to the different injection strategy of the blends in comparison to the one used for pure diesel. However, it is possible to see that O50D50 shows a heat release behavior more similar to D100. Therefore, the higher energy released between 15 and 30 CAD (around 50 to 80% of the total energy released) by blends with diesel content below 50% and pure OME_X cannot be explained by the different injection strategy. For this reason, it has been related with a higher soot oxidation rate during this stage, which is coherent with a faster burnout observed in the images and related to a faster decrease of soot concentration. It means that when diesel increases above 30%, the soot oxidation is worsened and the burnout process slowed down, which is confirmed by both natural luminosity and combustion heat release.

The increase of luminosity intensity due to the addition of diesel was evaluated by calculating and comparing the total accumulated radiation intensity of each blend at every measured CAD. The results are shown in Fig. 9. A logarithmic scale has been used to allow the comparison between all blends tested. The figure is representing a range of CADs where the maximum accumulated intensity is achieved. As it can be seen, only a 10% of diesel is enough to increase one order of magnitude the light intensity emitted by the flame. This could be linked with the soot formation increase caused by the diesel addition. As the percent of diesel added in the blend rises, the differences in terms of radiation intensity become higher. This behavior is very clear up to 30% of diesel blend, where the difference in terms of absolute value increases as diesel mass increases. However, for 50% of diesel, the differences in comparison with neat diesel (D100) are reduced. This suggests that the potential of OME_X to promote less soot formation has a minimum effect when diesel fraction increases above 50%. A similar behavior

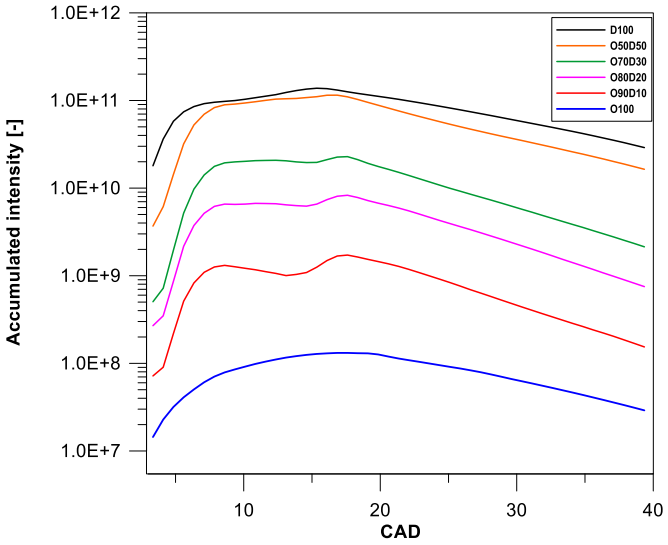

Fig. 9. Accumulated intensity for the different fuel blends (logarithmic scale).

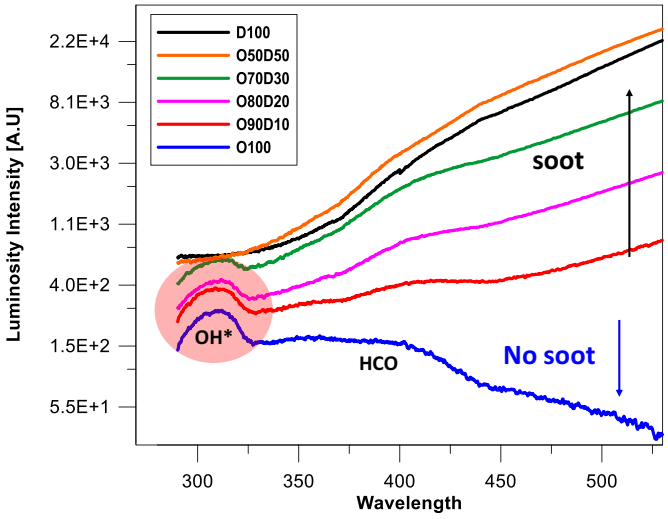

Fig. 10. Spectrum at 10 CAD for the different blends.

when using different diesel substitution rates in OME_X was found by Garcia, et al. [15] in a metal engine.

3.2. High speed spectroscopy

Despite it can be expected negligible soot formation by OME_X, in Fig. 8 and Fig. 9 it is possible to see that the combustion of this fuel emits broadband radiation. However, it must be highlighted that this signal includes the contribution of other sources different from soot. One of the most important is chemiluminescence. Although it is weak in comparison to soot thermal radiation, it becomes relevant when soot concentration is reduced, e.g. first or last stages of combustion or when using low sooting fuels like OME_X. Thus, based on natural luminosity imaging, it is difficult to state whether the radiation observed for this fuel is chemiluminescence or includes soot emission contributions.

These uncertainties affect not only pure OME_X but also the blends with low diesel content (specially O90D10). In order to properly identify the dominating radiation source for each fuel tested, the use of high-speed spectroscopy is proposed. In contrast with natural luminosity imaging, it is a spectrally resolved technique which allows to characterize not only radiation intensity but also the spectrum characteristics.

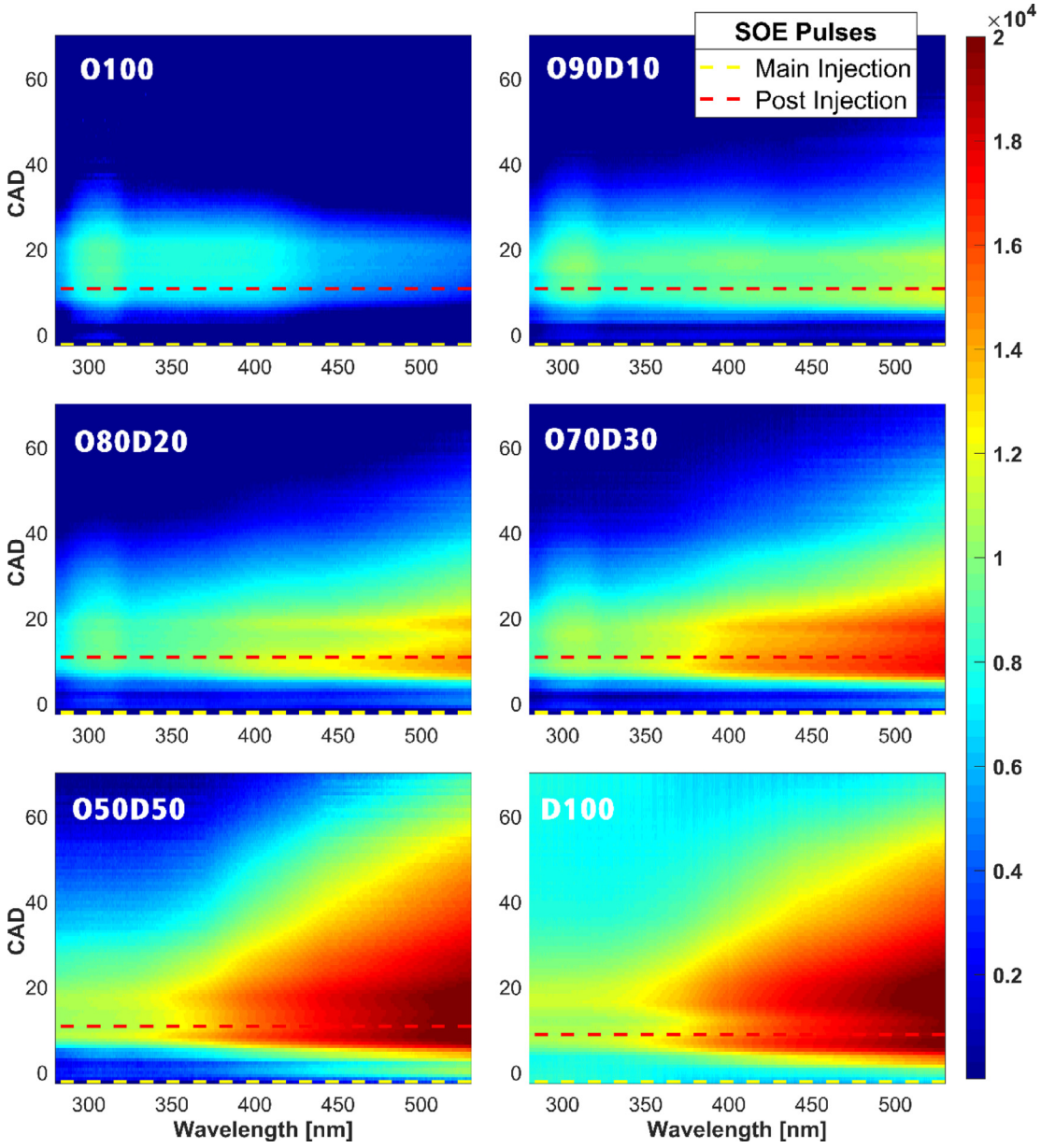

Fig. 11. Maps of the high-speed spectroscopy analysis for the different blends.

In order to highlight the differences among fuels, the spectra of the combustion process at 10 CAD are shown in Fig. 10, for all them. As it can be observed, O100 presents a completely different spectrum in comparison with the other blends. The maximum intensity in the spectrum comes from the OH* emissions. The peak of OH* is broad due to the presence of several optics between flame and camera and the large spectrograph slit aperture used for the tests, which was necessary to achieve enough sensitivity. From 420 nm, the light intensity starts to decrease rapidly, which confirms the non-soot formation. Up to 30% of diesel, the OH* chemiluminescence contribution can be identified in the spectra. From O50D50, the high soot formation increases and the OH* chemiluminescence signal disappears. In general, the light intensity and the slope of the curve increases in the visible range (450–500 nm) as the diesel concentration increases. This is a consequence of the higher soot formation.

The maps presented in Fig. 11 show the temporal evolution of the radiation spectrum during the combustion process of the different blends. Each map represents the wavelengths in the x-axis, from 290 nm to 530 nm. The y-axis represents the CAD evolution. The first thing that can be confirmed with this technique is the absence of soot during pure OME_X combustion. Soot thermal radiation is characterized by an exponential increase of the intensity towards higher wavelengths (in the range considered in this work). Thus, as this behavior is not observed for OME_X, it can be stated that no soot thermal radiation is detected. In contrast, it is possible to see at around 310 nm that the OH* chemiluminescence radiation is very intense during all combustion duration, from the earlier to the late combustion stages. During the first stages of the combustion process, the OH-radicals brake the precursors of the soot formation. In addition, the high oxygen content could increase the near-stoichiometric zones, increasing the concentration of OH*. Additionally, a continuum band, centered around 380 nm, is visible. It can be associated with the HCO radical (Vayda bands from 270 to 410 nm) [20], which represents the transition from the low to high temperatures reactions [21]. Therefore, based on the spectrum analysis, it can be stated that natural luminosity images represent mainly HCO emissions in the visible range (above 400 nm).

When diesel is mixed with OME_X, characteristic soot thermal radiation appears as it can be observed that the intensity increases with wavelength in the visible range. A 10% of diesel blended in OME_X is enough to generate soot. However, its concentration is low as its radiation is not dominating the emission spectrum. Additionally, it can be observed that thermal radiation disappears quickly (before 25 CAD) which suggests a fast soot oxidation. As the diesel content increases, more soot is generated and more difficult becomes its oxidation. Up to 20% of diesel, the soot formed during main and post injection can be easily distinguished. As it was observed with natural luminosity images, the soot radiation generated during the main injection drastically decreases. This suggesting a fast oxidation process before the start of the post injection event. From 30% of diesel, soot emission increases. Furthermore, when the post injection starts, the main injection radiation slightly decreases, evidencing a clear reduction of the oxidation rate at this stage of the combustion process. For O70D30, it is still possible to see an important OH* emission, which can be related with a high concentration of this radical. It helps on completely oxidizing soot before the piston achieves the 40 CAD.

When diesel fraction is increased to 50%, the behavior drastically changes. The characteristic OH* intensity peak observable in the blends until 30% of diesel cannot be identified for O50D50 and D100. This could be associated with two main factors. The first one is related with the intensifier settings used for these two fuels. The configuration guaranteed no saturation in the visible range (where soot thermal radiation is more intense) but the sensitivity in the UV-range was reduced. Therefore, the lower intensity of the OH* was not registered by the camera. The second factor is related with the attenuation of the OH* signal due to the high soot concentration during the diffusion phase. This effect was already discussed in a previous works [19,27]. The spectra of O50D50 and D100 also shows a similar soot formation and oxidation behavior. The radiation intensity levels are similar, and, in both cases, it is possible to see soot radiation up to 60 CAD. This confirms the trend observed with natural luminosity (Fig. 8) and the HR curve (Fig. 7). The higher slope of the curves for O50D50 and D100 suggest a higher chemical activity in comparison to the other blends late in the cycle. It can be concluded that the benefits of using OME_X seems to be reduce significantly when it represents less than 50% of the mixture.

As it has been described in the methodology section, the spectrograph information can be used to evaluate soot concentration. For this purpose, a 2-color pyrometry algorithm is applied to the radiation intensity at 450 and 530 nm, for all the blends and D100 (pure OME_X was excluded). Thus, an average soot KL evolution is calculated. Results are summarized in Fig. 12. For O90D10, the KL values were lower than the inferior limit (0.001) set for the calculation, confirming very low soot formation. For O80D20, the soot formed during de combustion process is higher and measurable. Nevertheless, it is still very low if compared with the remaining blends. The first remarkable KL increment is found between O80D20 and O70D30. Thus, it can be stated that above 20% of diesel fraction its effect on soot formation is relevant.

When comparing O50D50 and O70D30, it can be seen that, until 20 CAD, main differences are focused on the high peaks which correspond to the combustion of the main and post injection. These peaks are also visible for D100 but not for the blends with less diesel content. Additionally, a great difference can be noted during the oxidation phase, after 20 CAD. The soot of O70D30 oxidizes much faster than O50D50 as the KL values decreases faster. In fact, it is notorious that the blend with the highest diesel fraction O50D50 presents clear difficulties to oxidize soot.

When O50D50 is compared to D100, there are some important points to be highlighted. First of all, as shown in Fig. 5, the longer injection duration results in longer oxidation time for the blend in comparison to D100. In this case, although the soot formed during main and post-injection combustion is higher, the injection duration is much shorter and the oxidation process begins earlier. Additionally, it must be pointed out that as long as we move later in the cycle, temperature and pressure decrease which hinders the oxidation process. Another consideration is related with the similar light intensity presented in the spectroscopy and natural luminosity analysis between the two fuels. In a first approach, results suggested similar soot formation for both fuels. However, it must be kept in mind that soot thermal radiation intensity is related with its concentration but also with its temperature. In this sense, the 2-color pyrometry shows that soot formed by O50D50 is lower than D100. This indicates that the high light intensity of radiation is also caused by a higher temperature. The higher peak of RoHR, as shown in Fig. 6, could be increasing the temperature inside the combustion chamber in relation to the 100D.

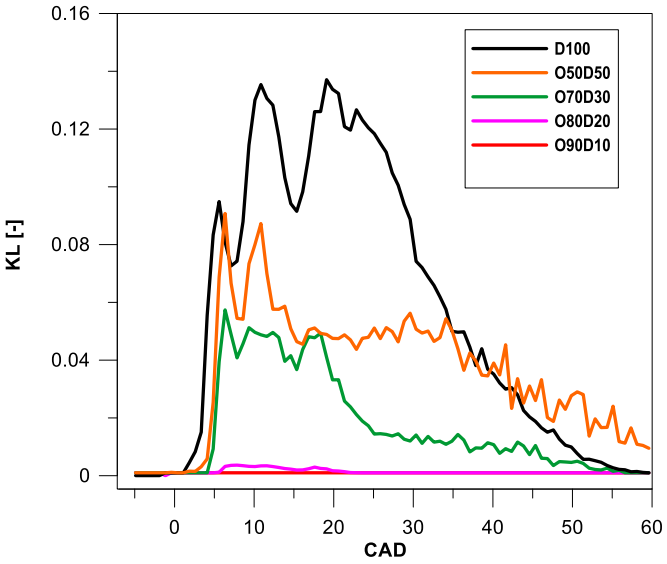

Fig. 12. KL values for the different OMEX-diesel blends.

The 2-color pyrometry allows to establish a relative comparison between blends. Based on these results, it can be stated that diesel can be added up to 20% of mass substitution rate without significantly increasing soot formation. An important soot reduction as well as an efficient oxidation process is still possible to obtain with 30% of diesel in comparison to pure diesel. However, above 50% of diesel, although soot formation is still lower than for 100D, higher soot levels reach later stages of the cycle as a consequence of the longer injections required. Thus, the potential benefits of improving soot oxidation disappear. To keep the same engine load, a trade-off exists between the capacity of OME_X to reduce soot formation and improve soot oxidation and the necessity of longer injection durations due to its lower LHV.

4. Conclusions

The combustion process as well as the soot formation for different OME_X-diesel blends have been studied in the current work, focusing on the influence of diesel substitution rate. Three different optical techniques were used for the analysis: natural luminosity, spectroscopy and 2-color pyrometry. Results can be summarized below:

- The cumulative heat release curves showed that above 30% of diesel content, the oxidation velocity considerably decreases and extends the burnout process.

- A 10% of diesel blend is enough for increasing in one order of magnitude the natural light intensity emitted by the flame. Up to 30% of diesel blend, the light intensity increases as the diesel mass quantity increases. Above 50% of diesel mass, the increment in terms of light intensity reduced significantly.
- The spectroscopy measurements have proven the absence of soot during pure OME_X combustion. As diesel mass is increased in the blend, the radiation for higher wavelengths (related to soot thermal radiation) increases as well.
- Significant OH^* emission could be appreciated for the blends with up to 30% of diesel mass. This can be related with a high concentration of this radical which helps oxidizing soot and its precursors before 40 CAD.
- 2C pyrometry shows that the soot formation can be kept very low up to 20% of diesel mass substitution rate. For 50% of diesel content, the soot reduction is still remarkable. However, the longer injection duration in comparison to pure diesel extends the late soot oxidation.

Declaration of Competing Interest

The authors declare that they have no known competing financial interests or personal relationships that could have appeared to influence the work reported in this paper.

Acknowledgments

The authors gratefully acknowledge the Generalitat Valenciana for partially supporting this work through the Programa Santiago Grisolía (GRISOLIAP/2018/142) program. In addition, Daniel Lérida for his laboratory work on the engine maintenance, operation, and control.

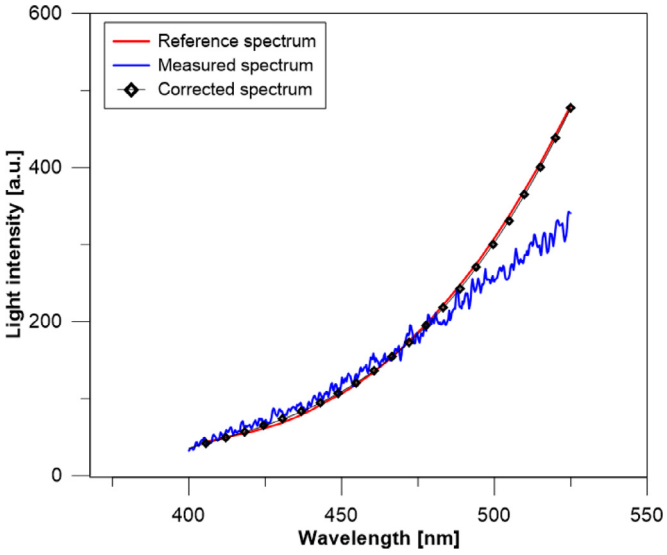

Fig. A2. Comparison between the tungsten-ribbon lamp measured spectrum (blue) with the grating centered at 470 nm, the one obtained after calibration (black) and the real spectrum (red).

Funding

This work was partially funded by Generalitat Valenciana through the Programa Santiago Grisolıá (GRISOLIAP/2018/142) program.

Appendix A

Spectroscopy image calibration

The signal registered by the high-speed camera that is coupled to the spectrograph needs to be calibrated in terms of wavelength

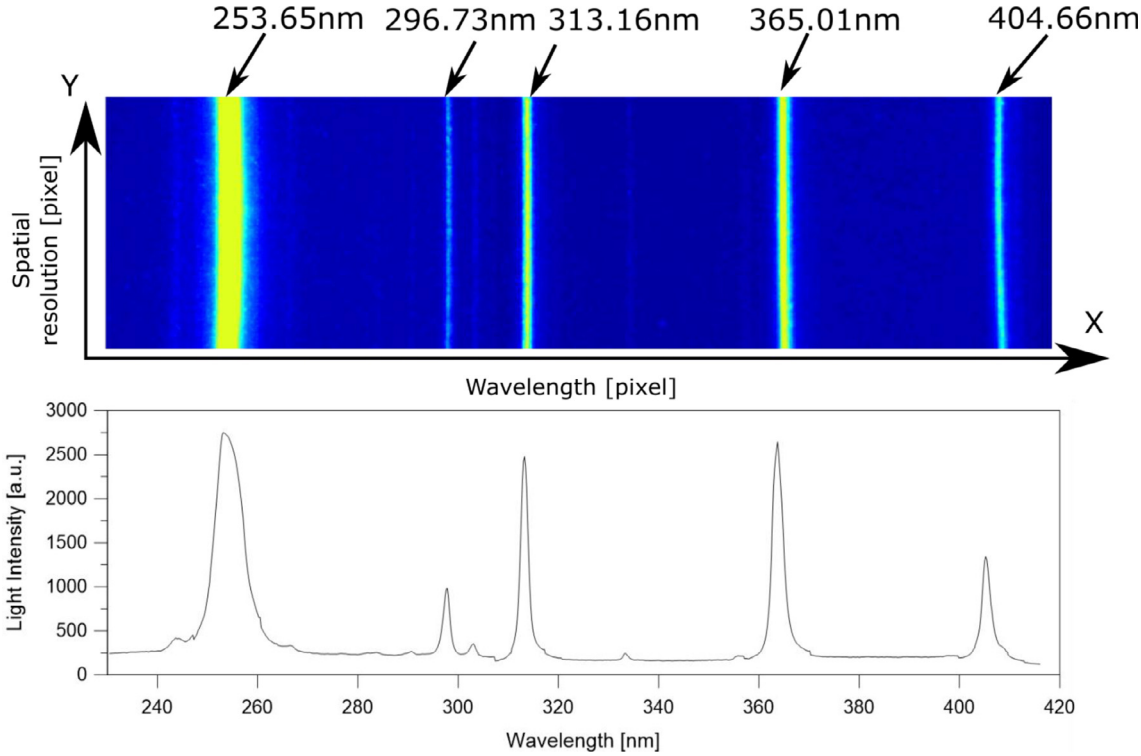

Fig. A1. Image of the emission spectrum of a calibration mercury – argon lamp (top) and the corresponding spectrum obtained by applying the first step of the calibration procedure. Information corresponds to the grating centered at 330 nm.

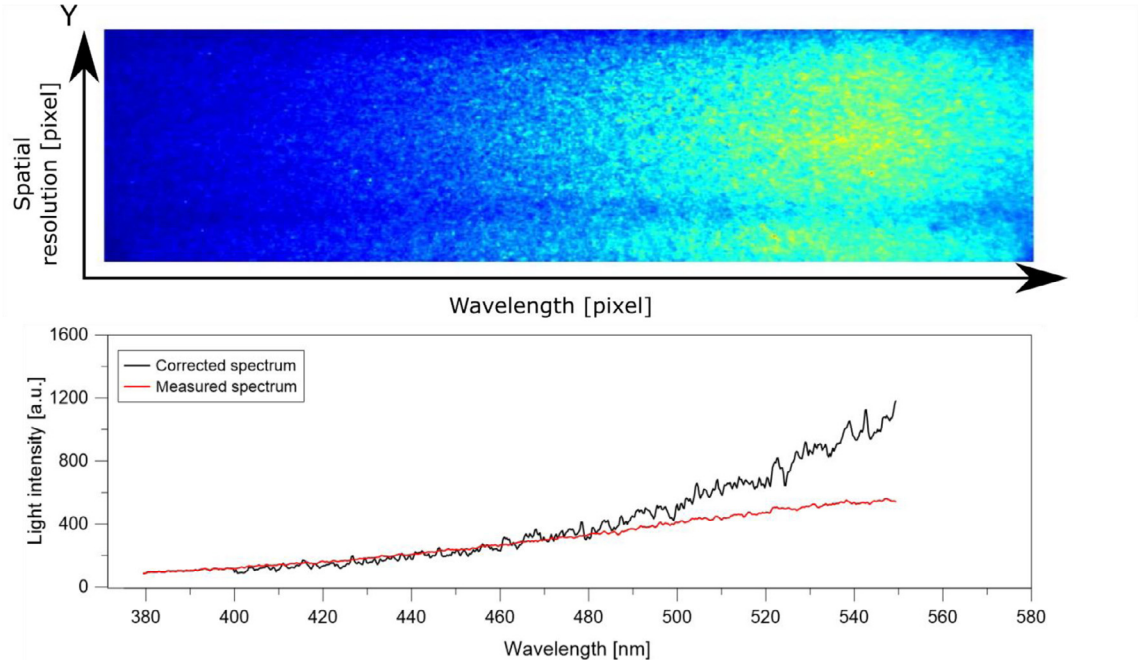

Fig. A3. Emission registered for pure Diesel with the grating centered at 470 nm (top) and the resulting spectrum (bottom) before and after the calibration procedure.

and intensity of radiation to obtain an accurate emission spectrum. In this work, a procedure was developed which is described in the following lines.

The Fig. A1 shows an example of the signal acquired, which corresponds to one of the tests performed in this work. For each image, the pixel coordinate in the x-axis is translated to the corresponding wavelength value (thanks to the calibration procedure). Additionally, for each column, all pixels are averaged to obtain a unique averaged intensity value per wavelength.

The first step of the process consists of translating the x-axis of each image capture by the high-speed camera to the corresponding wavelength value. For this purpose, the discrete emission spectrum of a Mercury – Argon was used. The emission bands of this equipment allow to stablish the correspondence between the x-axis position in the images and the corresponding wavelength, for all the grating positions used in this work. An example of this procedure is shown in Fig. A1, where the imagen registered by the high-speed camera (top) is compared with the spectrum obtained by averaging the pixel intensity in the y-axis and identifying the wavelength of the main peaks of the image.

The second step of the calibration procedure is focused on compensating the wavelength-dependent efficiency of the different optical elements and the grating. For this purpose, a tungsten-ribbon calibration lamp was used as reference [28]. This device presents thermal continuous emission spectrum, which was calibrated in laboratory providing the intensity of radiation (W/(sr m^2nm)) per wavelength. The signal registered by the high-speed camera corresponding to this device is compared to its calibrated spectrum, to define a wavelength-dependent correction factor. It is assumed that the efficiency at the central wavelength (where the grating is centered) is maximum. Then, the ratio between the signal at this wavelength and at any other wavelength must be equal to the ratio between the intensity of radiation of the lamp at the same wavelengths. Based on this, a calibration factor is calculated and applied to the registered spectrum. In Fig. A2, a comparison between the registered spectrum and the corrected one are shown. The real lamp emission spectrum has been included as reference, which has been normalized to be comparable with the measured spectrum. Data corresponds to a grating configuration centered at 470 nm. As it can be seen, the optical set-up efficiency is constant up to 450 nm. After this, the efficiency starts to decrease. However, the calibration procedure can compensate this change of behavior and the corrected spectrum is close to the reference one.

For each acquisition configuration (grating position, intensifier gain and shutter time), a specific wavelength-dependent correction factor needs to be calculated. Besides, it must be obtained using the same optical set-up as the one used in experiments. Otherwise, the efficiency of the optical elements not used in this procedure will not be considered in the correction factor and it will affect its accuracy.

In Fig. A3 it is shown an example of the calibration procedure applied to experimental data. It corresponds to pure diesel with the grating centered at 470 nm. The signal registered (top) is converted into an emission spectrum (bottom) applying the first step described in this appendix. Then, the correction coefficient calculated based on the tungsten-ribbon lamp (second step) is applied to compensate for the efficiency of each optical element including the spectrograph, the intensifier, and the camera (bottom).

The final step is to calculate a correlation between the intensity of radiation of the tungsten-ribbon lamp and the corresponding digital levels obtained by the optical set-up and the correction procedure described above. This correlation is applied to experimentally measured combustion spectra to transform them form digital levels to intensity of radiation and apply the 2C pyrometry algorithm.

References

[1] A. García, J. Monsalve-serrano, S. Martínez-boggio, Potential of hybrid powertrains in a variable compression ratio downsized turbocharged VVA Spark Ignition engine, Energy 195 (2020) 117039, doi:10.1016/j.energy.2020.117039.
[2] A. Omari, B. Heuser, S. Pischinger, C. Rüdinger, Potential of long-chain oxymethylene ether and oxymethylene ether-diesel blends for ultra-low emission engines, Appl. Energy 239 (2019) 1242–1249, doi:10.1016/j.apenergy.2019.02.035.
[3] C. Honecker, S. Glueck, Optical Spray Investigations On OME3-5 in a Constant Volume High Pressure Chamber, 2020, pp. 1–9, doi:10.4271/2019-24-0234. Abstract.

[4] Q. Yang, U. Stuttgart, M. Bargende, U. Stuttgart, The Application of E-Fuel Oxymethylene Ether OME1 in a Virtual Heavy-Duty Diesel Engine For Ultra-Low Emissions, 2020, pp. 1–10, doi:10.4271/2020-01-0349.Abstract.
[5] J. Burger, M. Siegert, E. Ströfer, H. Hasse, Poly (oxymethylene) dimethyl ethers as components of tailored diesel fuel : properties, synthesis and purification concepts, Fuel 89 (2010) 3315–3319, doi:10.1016/j.fuel.2010.05.014.
[6] A. Damyanov, P. Hofmann, B. Geringer, N. Schwaiger, T. Pichler, M. Siebenhofer, Biogenous ethers: production and operation in a diesel engine, Automot. Engine Technol. 3 (2018) 69–82, doi:10.1007/s41104-018-0028-x.
[7] H. Liu, Z. Wang, J. Wang, X. He, Improvement of emission characteristics and thermal efficiency in diesel engines by fueling gasoline/diesel/PODEn blends, Energy 97 (2016) 105–112, doi:10.1016/j.energy.2015.12.110.
[8] S.E. Iannuzzi, C. Barro, K. Boulouchos, J. Burger, Combustion behavior and soot formation/oxidation of oxygenated fuels in a cylindrical constant volume chamber, Fuel 167 (2016) 49–59, doi:10.1016/j.fuel.2015.11.060.
[9] H. Chen, X. Su, J. Li, X. Zhong, Effects of gasoline and polyoxymethylene dimethyl ethers blending in diesel on the combustion and emission of a common rail diesel engine, Energy 171 (2019) 981–999, doi:10.1016/j.energy.2019.01.089.
[10] M. Härtl, P. Seidenspinner, E. Jacob, G. Wachtmeister, Oxygenate screening on a heavy-duty diesel engine and emission characteristics of highly oxygenated oxymethylene ether fuel OME1, Fuel 153 (2015) 328–335, doi:10.1016/j.fuel.2015.03.012.
[11] D. Pélerin, K. Gaukel, M. Härtl, E. Jacob, G. Wachtmeister, Potentials to simplify the engine system using the alternative diesel fuels oxymethylene ether OME 1 and OME 3 – 6 on a heavy-duty engine, Fuel 259 (2020) 116231, doi:10.1016/j.fuel.2019.116231.
[12] C. Barro, M. Parravicini, K. Boulouchos, Neat polyoxymethylene dimethyl ether in a diesel engine ; part 1 : detailed combustion analysis, Fuel 256 (2019) 115892, doi:10.1016/j.fuel.2019.115892.
[13] A. Omari, B. Heuser, S. Pischinger, Potential of oxymethylenether-diesel blends for ultra-low emission engines, Fuel 209 (2017) 232–237, doi:10.1016/j.fuel.2017.07.107.
[14] P. Dworschak, V. Berger, Neat Oxymethylene Ethers: Combustion Performance and Emissions of OME 2, OME 3, OME 4 and OME 5 in a Single-Cylinder Diesel Engine, 2020, pp. 1–13, doi:10.4271/2020-01-0805.Abstract.
[15] A. García, A. Gil, J. Monsalve-serrano, R.L. Sari, OMEx-diesel blends as high reactivity fuel for ultra-low NOx and soot emissions in the dual-mode dual-fuel combustion strategy, Fuel 275 (2020) 117898, doi:10.1016/j.fuel.2020.117898.
[16] A. García, J. Monsalve-serrano, D. Villalta, R. Lago, V. Gordillo, P. Gaillard, Potential of e-Fischer Tropsch diesel and oxymethyl-ether (OMEx) as fuels for the dual-mode dual-fuel concept, Appl. Energy 253 (2019) 113622, doi:10.1016/j.apenergy.2019.113622.
[17] H. Liu, Z. Wang, Y. Li, Y. Zheng, T. He, J. Wang, Recent progress in the application in compression ignition engines and the synthesis technologies of polyoxymethylene dimethyl ethers, Appl. Energy 233–234 (2019) 599–611, doi:10.1016/j.apenergy.2018.10.064.
[18] A. Srna, C. Barro, K. Herrmann, F. Möri, R. Hutter, K. Boulouchos, POMDME as an alternative pilot fuel for dual-fuel engines: optical study in a RCEM and application in an automotive size dual-fuel diesel engine, SAE Tech. Pap. Ser. 1 (2018) 1–16, doi:10.4271/2018-01-1734.
[19] J.V. Pastor, A. García, C. Micó, F. Lewiski, An optical investigation of Fischer-Tropsch diesel and Oxymethylene dimethyl ether impact on combustion process for CI engines, Appl. Energy 260 (2020) 114238, doi:10.1016/j.apenergy.2019.114238.
[20] E. Mancaruso, B.M. Vaglieco, Spectroscopic measurements of premixed combustion in diesel engine, Fuel 90 (2011) 511–520, doi:10.1016/j.fuel.2010.09.052.
[21] J.V. Pastor, J.M. García-Oliver, A. García, C. Micó, R. Durrett, A spectroscopy study of gasoline partially premixed compression ignition spark assisted combustion, Appl. Energy 104 (2013) 568–575, doi:10.1016/j.apenergy.2012.11.030.
[22] Hwang W., Dec J., Sjöberg M. Spectroscopic and chemical-kinetic analysis of the phases of HCCI autoignition and combustion for single- and two-stage ignition fuels 2008;154:387–409. https://doi.org/10.1016/j.combustflame.2008.03.019.
[23] J.V. Pastor, A. García, C. Micó, S. Möller, J.M. García-Oliver, Application of optical diagnostics to the quantification of soot in n -alkane flames under diesel conditions, Combust. Flame 164 (2015) 212–223, doi:10.1016/j.combustflame.2015.11.018.
[24] L. Pellegrini, M. Marchionna, R. Patrini, C. Beatrice, N. Del Giacomo, C. Guido, Combustion behaviour and emission performance of neat and blended polyoxymethylene dimethyl ethers in a light-duty diesel engine, SAE Tech. Pap. Ser. 1 (2012), doi:10.4271/2012-01-1053.
[25] L. Rao, Y. Zhang, D. Kim, H.C. Su, S. Kook, K.S. Kim, et al., Effect of after injections on late cycle soot oxidation in a small-bore diesel engine, Combust. Flame 191 (2018) 513–526, doi:10.1016/j.combustflame.2018.02.014.
[26] J. Pastor, P. Olmeda, J. Martín, F. Lewiski, Methodology for optical engine characterization by means of the combination of experimental and modeling techniques, Appl. Sci. 8 (2018) 2571, doi:10.3390/app8122571.
[27] S.S. Merola, C. Tornatore, G. Valentino, L. Marchitto, UV-Visible Imaging and Natural Emission Spectroscopy of Premixed Combustion in High Swirl Multi-Jets Compression Ignition Engine Fuelled with Diesel-Gasoline Blend, 2020, doi:10.4271/2012-01-1723.
[28] T. Xuan, J.V. Pastor, J.M. García-Oliver, A. García, Z. He, Q. Wang, et al., In-flame soot quantification of diesel sprays under sooting/non-sooting critical conditions in an optical engine, Appl. Therm. Eng. 149 (2019) 1–10, doi:10.1016/j.applthermaleng.2018.11.112.